On the heterogeneous nature of deformation in a strain-transformable beta metastable Ti-V-Cr-Al alloy

Lola Lilensten, Y. Danard, C. Brozek, S. Mantri, P. Castany, T. Gloriant, P. Vermaut, F. Sun, R. Banerjee, F. Prima

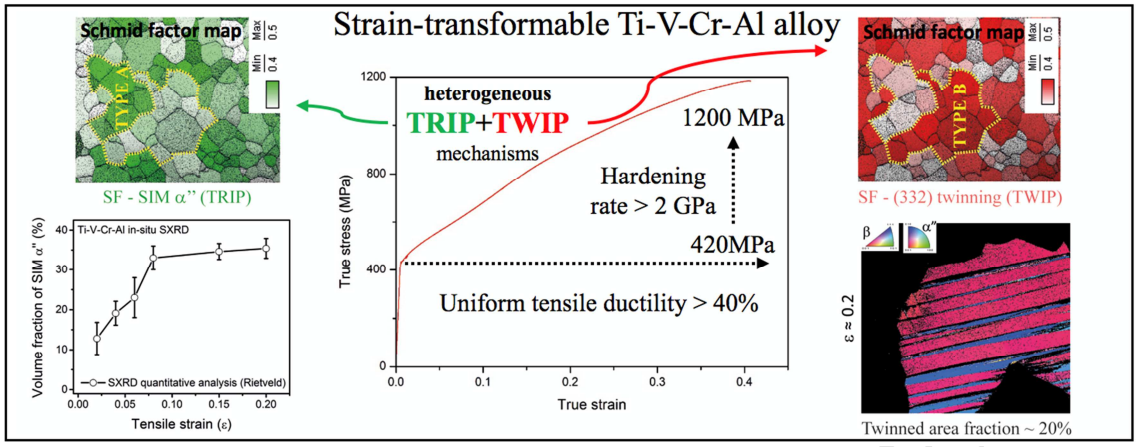

On the heterogeneous nature of deformation in a strain-transformable beta metastable Ti-V-Cr-Al alloy

L. Lilensten[a,1], Y. Danard[a], C. Brozek[a,2], S. Mantri[b], P. Castany[c], T. Gloriant[c], P. Vermaut[a], F. Sun[a]*, R. Banerjee[b], F. Prima[a]

[a]: PSL Research University, Chimie ParisTech-CNRS, Institut de Recherche de Chimie Paris, 75005 PARIS, France.

[b]: Department of Materials Science and Engineering, University of North Texas, Denton, TX-76207, USA

[c]: Univ Rennes, INSA Rennes, CNRS, ISCR – UMR 6226, F-35000 Rennes, France

[1]: present address: Department of Microstructure Physics and Alloy Design, Max-Planck-Institut für Eisenforschung GmbH, 40237, Düsseldorf, Germany

[2]: present address: Eramet Research, 1 rue Albert Einstein, 78193 Trappes, France

*: corresponding author fan.sun@chimie-paristech.fr

Abstract

Ti-10V-4Cr-1Al wt% (TVCA) is a new grade of titanium alloy, developed to combine twinning induced plasticity (TWIP) and transformation induced plasticity (TRIP) effects. The TVCA alloy exhibits a very high strain-hardening rate and an excellent balance between strength and ductility for great potential in aerospace applications. Deformation mechanisms are investigated using in-situ techniques as synchrotron X-ray diffraction (SXRD) and in-situ electron backscatter diffraction (EBSD) analysis during

tensile strain, as well as transmission electron microscopy (TEM). The results reveal that permanent {332}<113> mechanical twinning and an unstable orthorhombic α" martensite are the major deformation products. This study aims at unveiling the interaction and co-deformation of the various deformation features, that lead to the outstanding mechanical properties of the alloy. The very high strain hardening rate could be explained by the simultaneous activation of two different deformation modes, the primary TRIP mode on one side, and the hybrid TWIP and secondary TRIP mode on the other one, in different grains, resulting in in-grain dynamic hardening (Hall-Petch) / softening (α" martensite) effects and meso-scale dynamic mechanical contrast. Selection of the deformation mechanism – TRIP or TWIP –, which seems to be inhomogeneous, at both the inter- and the intra-granular level, is investigated.

Keywords

Titanium alloy, deformation twinning, martensitic phase transformation, strain hardening, deformation structures

1. Introduction

The development of β-titanium alloys has attracted an increasing attention over the last few years for fulfilling the growing demand from the aerospace industry. Until recently, the interest brought to this family of titanium alloys was limited because of their rather weak work hardening and ductility, specific to bcc structures. However, proof was given that triggering twinning and/or martensitic phase transformation in the β-phase under

applied stress, even for dual-phase alloys, could greatly enhance both the work hardening capability as well as the elongation of the alloy, leading to materials with great potential for various applications [1–9]. It is now well known that the transformation induced plasticity (TRIP) and the twinning induced plasticity (TWIP) effects are closely related to the chemical stability of the β-phase at room temperature [10]. The stability domains of the later can be predicted with good accuracy using the Bo-Md (where Bo stands for mean bond order and Md for mean d-orbital energy) design method [2,11], DFT [12], but also Calphad approach. They allow to target the boundaries of the stable β domains, where TRIP and TWIP are more likely to occur. The understanding of the deformation mechanisms, taken independently, benefits from several studies. Concerning the TRIP effect, a good understanding of the formation of stress induced martensite was reached with the study of shape memory alloys, superelastic alloys and gum-metals, used for biomedical applications [4,5,8,13,14]. As for the twinning effect, it has been investigated on various aspects, such as the influence of the grain orientation [15–17], deformation rate [18] and chemical homogeneity [19]. Twinning mechanisms for the bcc structure are still in hypotheses among various models, especially regarding the {332}<113> twinning, theoretically unfavorable yet widely observed in metastable β-Ti-alloys [20–23]. Recent assumptions based on experimental observations suggest that the {332}<113> twinning process could be mediated by the formation of orthorhombic martensite, formed as a martensitic reversion product [23–25]. This shows the complexity of the interactions between the

various phenomena, and how interdependent they could be.

Thus, even more complex than single TWIP or single TRIP effects, the interplay of the two deformation modes in TWIP/TRIP alloys, although leading to highly desirable mechanical properties, remains far from being well understood; even if some first attempts to describe the deformation sequence and the interactions between the various features (including the role of the stress induced ω-phase, not observed in this study) have been reported [1,26–28]. Yet, no agreement on the deformation sequence was found, and microstructural mechanisms are derived mainly based on post-mortem imaging, limiting the understanding of the complex interactions which are very sensitive to stress-strain environment [26,29,30]. This study focuses on the *in-situ* investigation of the deformation mechanisms at the various length scales, and their interaction, using a Ti-V-Cr-Al alloy designed from d-electron approach [2,11]. The composition is designed for the formation of TRIP and TWIP upon deformation, using Bo (mean bond order) and Md (mean *d*-orbital energy) parameters of 2.785 and 2.353 respectively [2,11,31]. *In-situ* analyses are of particular interest in this case, considering the partially reversible (when tensile stress is released) behavior of the martensite. A special focus is given to the understanding of the criteria ruling the selection of the deformation mechanisms, to try to add to the existing results on the "deformation sequence" in such alloys. The macro-scale data (*in-situ* synchrotron X ray diffraction SXRD) and the microstructural analyses (*in-situ* SEM and EBSD, with supplementary TEM) are used to investigate the evolution of the martensitic and the β-twins fractions.

The triggering of one and/or the other mechanism – among TRIP and TWIP - for the various grains, using a Schmid factor (SF) analysis, is used to explain the exceptional tensile properties of the material.

2. Experimental

Ti-10V-4Cr-1Al alloy (TVCA) in wt% is processed by arc melting under a high Ar purity atmosphere. A 200g ingot is melted using industrial purity Ti sponges, Cr granules, a master alloy of AlV and Al shots. Plates of 3mm thickness are cut out, homogenized at 1173K under air for 900 s and then water quenched. Slice-cut samples are cold rolled down to 0.5mm sheets, corresponding to a reduction level of 80%. To restore a fully β state, cold rolled sheets are finally solution treated (ST) under high purity Ar atmosphere at 1033 K for 900 s, and then water quenched. Tensile tests are performed at room temperature using an INSTRON5966 machine with an extensometer, on specimen with dimensions of 50 mm x 5 mm x 0.5mm, at a strain rate of 10^{-3} s^{-1}. *In-situ* SEM tensile samples, with dimensions 35 mm x 2mm x 0.5mm, are prepared by electropolishing. Electron backscatter diffraction (EBSD) scans are collected using a field emission gun scanning electron microscope operating at 20kV, with step size ranging from 0.5 to 0.01µm. *In-situ* tensile tests are performed using a Proxima 100-Micromecha machine. Deformation is followed by secondary electron (SE) imaging during the loading state and EBSD scans are recorded at different strains. Because of some surface relief related to the activated deformation mechanisms, preventing indexation, a few microns of the surface at the rupture stage were

electropolished before recording the last EBSD scan.

In situ SXRD is conducted at the high resolution beam line ID22 of the European Synchrotron Radiation Source (ESRF), Grenoble, France, from a tensile sample with gauge width of 4mm and 0.5mm in thickness. The incident X-ray beam had a diameter of 1 mm and a wavelength of 0.040002106 nm. Data collection of transmitted diffracted beams was performed over the 2θ angular range 6-24°, with a step size of 0.005°. Six scanning stages are carried out at room temperature, starting from the unloaded state, and then for increasingly loaded states, up to a strain of 0.20 with a strain rate of 10^{-4} s^{-1}. Analysis of the diffraction patterns consists in identifying the phases corresponding to the different peaks, and then estimating the lattice parameters owing to Pawley refinement using the TOPAS software. Estimation of the intensity of specific peaks is also carried out. Site-specific samples for transmission electron microscopy (TEM) were prepared using a FEI Nova NanoLab 200™ focused ion beam (FIB) system. TEM studies were carried out using a FEI Tecnai F20-FEG operating at 200 kV and FEI Tecnai G2 30 TWIN operating at 300 kV.

3. Results

3.1 Mechanical performances of Ti-V-Cr-Al alloy

The mechanical behavior is shown in form of a uniaxial tensile curve in figure 1a, in which a stable plastic flow starts at about 420MPa and is maintained until 1200MPa. Initiation of localized necking is observed at about ε=0.35, yet the total engineering elongation exceeds 50%. Consistent with the Bo/Md design strategy, the TVCA alloy

displays a complex, non-monotonic, stress-strain profile previously observed in both Ti-12Mo and Ti-8.5Cr-1.5Sn alloys, especially due to the hump in the work-hardening rate curve (figure 1b). The work hardening rate of TVCA reaches a maximum of about 2.6 GPa at ε=0.12. The vertex divides the work hardening process into two stages: early stage - from yielding to ε=0.12 - and late stage from 0.12 to 0.35. The work hardening rate is characterized by an increase in the early stages before to slowly decrease during the late stage.

3.2 *In situ* SXRD investigation of deformation mechanisms

Before deformation (ε=0), the single β phase (body center cubic bcc) with cell parameter a=3.26 Å is confirmed by SXRD (Figure 2). SIM is, as expected, triggered at the end of the elastic regime. The orthorhombic α" martensitic phase is indeed detected by the first SXRD analysis in tension, for a deformation of ε=0.02 (Fig. 2a), with lattice parameters a=3.06 Å, b=4.88 Å and c=4.62 Å determined by Rierveld refinement. The evolution of the volume fraction of α" is estimated from the quantitative Rietveld refinement results for each diffraction diagram, assuming that the texture is random (Figure 2b). Although this last hypothesis is a bit strong, it allows us to access approximately the amount of α'', as well as to get the relative evolution of the α'' phase fraction with strain. The volume fraction increases rapidly to about 30 vol% at at ε≈0.08, and then reaches a plateau, during which the amount increases very little, to reach approximately 35 vol% at ε=0.2.

3.3 Local analysis of the deformation mechanisms: a heterogeneous behavior

At the macro-scale, an EBSD analysis of the microstructure (Figure 3) reveals a 100% β structure prior deformation, consistently with the SXRD information, and an average grain size of 46 microns. The color code refers to the calculated SF of the {332}<113> twinning (in red) and to the one of the SIM formation, in green, calculated using the habit plane of the martensite. One can see that the grains are grouped, defining some zones that are more likely, based on the SF, to deform either by twinning or by formation of martensite. It can also be noted that when the grains are well oriented for one mechanism, the other mechanism is rather unlikely to occur. Therefore, further analyses were performed to identify the respective sequence of deformation mechanisms in the two populations of grains. The two populations are referred to in the following as “type A” grains, displaying high SF for SIM (TRIP), and “type B” grains displaying high SF for mechanical twinning (TWIP effect),

3.3.1 Deformation induced martensitic phase transformation (“Type A” grain)

For further investigation, a model “type A” grain is selected, and called grain A in the following. Plate-like deformation bands (Fig. 4a) are observed by SEI (secondary electron imaging) after *in-situ* tensile loading to ε=0.03. EBSD mapping identifies the nature of the bands as α” martensite. It can be seen from Fig. 4a that one of the bands is composed of two orientations of α” that are in twinning relationship. The orientation relationships between the α” phase variants and β matrix are verified by pole figure projection (Fig. 4c and 4d). The classical Burgers relationship $(110)_{\alpha''}$// $(2\text{-}11)_{\beta}$ is found

for the major SIM variant (green), but not found for purple one, confirming that the purple variant is obtained by twinning of the primary martensite (green variant). After releasing the tensile load, the martensite disappears (Fig. 4b), and a full β structure is restored, confirmed by EBSD mapping on the same zone. It shows that the martensitic phase transformation can be reversible in the early stage. In contrast, no mechanical twinning of beta phase was observed in the area for these deformation levels.

3.3.2 Stress induced twinning and secondary SIM ("Type B" grain)

In-situ SEM investigations are then performed to monitor the deformation of a grain, showing a high SF for mechanical twinning, denoted by Grain B hereafter.

SEI show that at yield (Fig. 5b), two straight parallel bands appear on the surface of Grain B, growing about 76° away from the tensile direction (vertical). At lower deformation (up to ε≈0.2), deformation seems to proceed by band multiplication, before thickening of the bands takes over.

Deformation strain is held at ε≈0.1 and ε≈0.2 for EBSD mapping, and a final EBSD is performed on the fractured sample (ε≈0.35). Phase maps are over imposed on the SE images (figure 5), and details of the orientation maps at the different stages can be found in the supplementary materials. Difficulties of indexation are noticed at the interfaces between bands and matrix, probably due to the shadow of the relief or to very fine and strained microstructures. The in-depth analysis of the nature of the deformation products, their orientation and surface fraction in the sample after rupture is then performed, and the results are given in Fig. 6a. For an easier identification, they are

labelled T1 to T4 for the β-twins, and a1 to a3 for the martensitic variants.

As can be seen in figures 5 and 6, the strain-induced deformation bands are mainly identified as β twins belonging to the {332}<113> twinning system (three twinning systems T1, T2 and T3, for a total surface fraction of 27.2%). A major twinning system T1 is observed, and one {112}<111> twin (T4) is formed at the late stage of the deformation (Figure 1 of supplementaty material), with low surface fraction of 0.7%. Some martensite is detected too, mostly on the right side of the grain. Three α" variants are found, with surface fractions of 2.3%, 1.3% and 6.7%. The a3 variant, it is the only one detected only after rupture (Figure 1 of supplementary materials), unlike the other variants which are identified for lower strains.

Considering the indexed parts, the {332} twins possess a higher volume fraction than the martensitic phase. The martensite surface area is also much lower than macroscopic SXRD estimation (Fig. 2b). Yet, this is a local result, and an analysis of this zone with lower magnification leads to 22.9% (surface fraction) of martensite at failure, closer to the SXRD results (Figure 2 of supplementary material). By plotting the stereographic projections of the different features (Figure 6c-e), classical crystallographic relationships are confirmed for the major T1 and the matrix, and for a1 variant and T1 but not for a1 and the matrix. This leads to the hypothesis that a1 is a secondary deformation product obtained from the deformation of T1 and not the matrix. Similar results are found for a2, that does not fulfill the Burgers relationship with the matrix but with T1 (not displayed here).

3.3.3 Detailed microstructures of twins and martensite

An in-band microstructure is studied by TEM, to try to better understand the complexity of the secondary deformation mechanisms and the underlying phenomena. Grain B is selected, and the lift-out is performed after fracture, on a band with low confidence of index (black pixels in Fig. 7a). Figure 7 shows the cross section of the band, where a step is observed at the surface. It is evidenced from the SAED patterns (Fig. 7b) that the microstructure is composed of a {332} twin with internal secondary α" phase. However, the α" phase seems unstable, since SAED pattern on the left of the Figure 7b, taken on the same area after six months of "aging" at room temperature, shows that the α" phase is actually reversed into its parent phase, the β {332} twin.

3.3.4 Schmid factor analysis

Details of the SF, that led to the selection of grains A and B as model grains, are given in Figure 8. It is completed with analysis of the experimentally observed deformation features (highlighted) and details of T1 are also given, as this system was shown to display internal secondary deformation features. The SF for the three best-oriented variants (highest SF) of {332} twins, {112} twins and α'' martensite are given. In all the cases, there is a {112} twinning system which displays the highest SF of all systems. However, such twins are not observed, except in grain B, for large strains (detected only in the last EBSD mapping). Apart from this twinning system, the mechanisms triggered in grains A and B fulfill the SF selection criterion: the formation of martensite is the favored mechanism in grain A and is indeed experimentally observed, similar to the

{332} twinning system for grain B, with the highest SF of 0.459 for the main variant T1 (3-23) [131]. The fact that the SF of martensite is not the highest one for the secondary deformation mechanism in T1, and yet it is the mechanism observed, may indicate that the SF rule is not respected for secondary deformation mechanisms. This is in line with the idea that secondary deformation mechanisms accommodate the mechanical contrast inside the grains, without any direct link with the macroscopic strain.

3.4 Correlation between the mechanical data and the analysis of the deformation mechanisms

Finally, the comparison between strain hardening rate and strain transforming products at two different scales is shown in Figure 9. In Figure 9a, results from macroscopic measurements, strain hardening from tensile test and α'' fraction from in-situ SXRD, are plotted as a function of tensile strain. The plateau reached by the martensitic fraction happens to correspond to the hump in the work-hardening rate. Microscopic evolutions of the area fractions of β twins and α" martensite in grain B (TWIP/TRIP mode) are presented in Figure 9b as a function of tensile strain. The increase in the twinned fraction is monotonic up to about 25 area% at rupture. In contrary the α'' fraction is very low and increases slowly until 20% and then strongly at the fractured stage. The difference between macroscopic and microscopic observations may confirm the preferential selection of local deformation mechanism according to the grain orientation.

4. Discussion

The tensile behavior coupled with *in-situ* analysis of the deformation mechanisms of a β-metastable Ti-alloy are reported in this paper. As expected from the shape of the tensile curve, a signature of strain transformable alloys with deformation processes related to TRIP and TWIP, stress induced martensite and twins are formed upon deformation, as indicated by the SXRD (Figure 2), SEM (EBSD) (Figure 4-6) and TEM analyses (Figure 7). Yet, an EBSD analysis at the macro-scale prior deformation suggests that, depending on their orientation and so their Schmid factor, some grains may be more favorable for TRIP and some other for TWIP. This could indicate that, rather than the existence of a unique deformation sequence in the alloy, each type of grain undergoes a different pattern. Therefore, the following discussion will focus on the "type A" and the "type B" ones. The different roles of the martensite, in the earlier deformation stage and in the late one, will be also discussed. Finally, the impact of this contrast, between the two populations of grains, will be discussed in the light of the mechanical properties and possible hardening mechanisms.

4.1 Investigation of the different behaviors observed in type A and type B grains

4.1.1 Selection of the primary deformation mechanism

The textural influence on mechanical twinning has been highlighted in several papers, through Schmid factor (SF) analysis [15–17]. However, this particular parameter has not been evaluated in case of potentially combined TRIP and TWIP effects, with subsequent questions on the twins/martensite interactions. As can be seen in Figure 2, the β-grains at the initial state seem to be, based on the calculation of the SF, well

oriented for one or the other mechanism, either TRIP or TWIP. Experimentally, it is confirmed that SF predicts with good accuracy which grain will TRIP or TWIP (at least as primary deformation mechanism). “Type A” grains, as the one investigated in figure 4, shows that the first deformation mechanism observed is TRIP, in good agreement with the calculation of the SF (Figure 8). In this grain, up to ε=0.03, no twinning of the β-phase is found.

Similarly, in the grain investigated in figures 5-7 (“type B” grain), TWIP is the primary deformation mechanism, with the formation and multiplication of {332}<113> twins in the first stage. In grain B, the detected martensite is identified as a secondary deformation product (discussed later in section 4.1.2). At the end of the deformation process, up to 30% (surface fraction) of the grain is twinned, and less than 10% is indexed as martensite, well below the average value of 35% calculated on the macroscopic level by SXRD. This highlights the fact that different behaviors are found at the grain-size level, and the macroscopic data only cannot reflect on the variety and complexity of the local behaviors. Therefore, the history of the deformation, applying in every grain, cannot be treated as unique, but must be split into at least two stories, for the type A and type B grains in the alloy. The fact that both mechanisms can be triggered as primary deformation mechanisms also indicates that the critical resolved shear stresses (CRSS) required for TRIP and TWIP are similar, as is classically expected for TRIP/TWIP alloys. Indeed, if one of the mechanisms had a much lower CRSS, it would be triggered regardless of the grain orientation.

4.1.2 Formation of secondary deformation products

When increasing the strain in grain B (figures 5-7), deformation products other than {332}<113> twinning are observed: {112}<111> twinning is found, as well as martensite variants. The fact that {112}<111> twinning is not observed earlier in the alloy (see supplementary material for details), in spite of its high SF (Figure 8) may be explained by a possible high CRSS, that prevented its earlier formation. Regarding the martensite, the indexed variants a1 and a2 do not fulfill the Burgers relationship with the matrix but with T1 (Figure 7d), therefore they can be identified as a secondary deformation mechanism.

Taking a closer look at the location where the martensite is formed, it seems to mostly be coupled with other features, such as a grain boundary or a {332} twin, with sometimes a very intricate structure for the latter case. This suggests that martensite is triggered at late deformation stages in the highly strained areas, to accommodate strong local strain fields.

Bands composed only of martensite (fully martensitic needles) are not found in this grain. Contrary to a1 and a2, detected at $\varepsilon=0.1$ and $\varepsilon=0.2$ in association with T1, a3 is observed in grain B only after rupture. This green variant, detected in several zones of grain B, has a twinning relationship with a1 and a2, and also a negative SF. This leads to the hypothesis that a3 is formed by twinning of a2 (previously indexed in the same zone in the grain), aiming at accommodating the backstress in the sample.

4.1.3 On the {332}<113> twinning

The formation of {332}<113> twins has been subjected to a lot of hypothesis, including shuffling, or martensitic mediation [23–25]. Yet, the controversy remains, as no "universal mechanism" is reached, each alloy presenting its own characteristic features. For this alloy, to get a better understanding of how the defects form and interact together, one of the band, that is not easily indexed, of the fractured sample, was looked at by TEM. One deformation step before, parts on the right side of the band was indexed as martensite (a1), and the left side of the band was indexed as T1.

Bright field images show that the band is actually composed of several components stacked on top of each other. The central and largest band was unambiguously indexed as orthorhombic martensite in (310) zone axis. It is surrounded by one band with {332}<113> twinning orientation relationship on each side, making the transition with the matrix.

This result is the opposite of what was observed in several papers [23–25], where the boundary between a {332}<113> twin and the matrix was made of orthorhombic martensite, more or less well defined. Results from the literature lead to the hypothesis that the formation of {332}<113> twins could be mediated by martensitic phase transformation. In the present case, several hints suggest that this scenario is not happening. First, the martensite is contained in the twin. Besides, the interface between the martensite and the twin is not parallel to the interface between the twin and the matrix. This indicates that the twin formed first, and that the martensite is a deformation sub-product, in good agreement with the EBSD data. Finally, the sample was analyzed

again after 6 months at room temperature ("aged" diffraction pattern in figure 7). The new TEM analysis of the "aged" sample shows that the martensite needle has transformed back into a bcc structure, the latter having the same orientation as the neighboring twin, and not the matrix. The martensite therefore reverted into its parent structure: the {332}<113> twin.

The deformation sequence observed here does not aim at being universal, since it is important to keep in mind that all the Ti β-metastable alloys with different compositions have a different sensitivity for the TRIP and the TWIP mechanism. But it shows that the mechanisms suggested, the martensitic mediation of twinning, although undeniable in the reported cases, also cannot be extended to the {332}<113> in general.

4.2 Understanding the deformation mechanisms

4.2.1 Correlation between the microstructural investigations and the tensile testing curve

Figure 1 shows that the tensile behavior can be seen as made of two different domains. The first one goes up to about $\varepsilon \approx 0.12$, and the second one goes from that point on. In the first stage, the work-hardening rate increases a lot, and decreases in the second one.

The first deformation stage is also marked by a strong increase of the quantity of martensite, as indicated by the SXRD data (figure 2), showing a raise from 0% (initial state, undeformed sample) to about 30%. The shape of the tensile curve is characteristic of alloys forming SIM with the double yielding, observed between $\varepsilon \approx 0.055$ and $\varepsilon \approx 0.12$. It is usually considered that the second yielding corresponds to the elastic deformation

of the martensite that was formed during the first stage (here up to $\varepsilon \approx 0.055$). This is in good agreement with the fact that according to SXRD data, the fraction of martensite in the material reaches a plateau at about 10% of deformation, which corresponds to the beginning of the hump in the work-hardening rate. Yet, as the present alloy is not purely superelastic but TRIP/TWIP, the mechanisms associated with this step combines elastic deformation of the martensite, but also twinning and dislocation glide.

The first deformation domain therefore seems to be controlled by two “independent” primary deformation mechanisms, twinning and SIM, each of them occurring in different grains (type A and type B).

During the second deformation stage, the amount of martensite increases very little. Considering this slight increase and the discussion of the previous part, it can be assumed that the martensite formed during that stage is a secondary deformation product, and is formed to accommodate local stress fields, explaining the much smaller quantity. This also explains the rather heterogeneous repartition of the martensite in the grain, mostly localized in the twins or at the grain boundaries, which are locations expected to be under higher strain levels.

4.2.2 Towards a two-levels composite effect

The study of the grains A and B brought a lot of information on the various behaviors observed in the grains. The first major point is that there is a heterogeneity between the grains depending on their orientation. Some of them are more favorably oriented for TRIP and some others for TWIP, therefore grains deforming by TWIP are lying next to

grains deforming by TRIP. However, the consequence of one or the other mechanism is not the same from a mechanical point of view. In type-B grains, the refinement of the microstructure by twinning creates hardening via the dynamic Hall-Petch law [32]. Twin boundaries act as barriers to gliding dislocations, consequently reducing their mean free path, and these grains harden. In comparison, the role of martensite is still under discussion, as it is classically considered as a soft phase, with a modulus lower than the one of the bcc phase. Besides, as was shown in a recent study, martensite may not act as a strong barrier for gliding dislocations, in comparison with twin boundaries [33]. It could however participate in the hardening by acting as dislocation source, and still contribute to hindering the dislocation glide. Overall, the hardening is expected to be different in type-A grains and type-B grains, leading to a first grain-level type of heterogeneities. The second point is that in type B grains (favorable for TWIP), martensite can form to accommodate the strong local strain fields, at twins or at grain boundaries, that may otherwise lead to earlier failure of the sample. Therefore, heterogeneities are observed at two different levels. The first one is the level of individual grains or groups of grains, and the second one is the intragranular scale. Thus, the distinct yet complementary roles of the two main deformation mechanisms TRIP and TWIP in type A and B grains may be used to explain the outstanding ductility and UTS in this alloy. It is well known that both mechanisms, taken individually or together, allow the beta structures to reach better mechanical properties, compared to simple dislocation glide [7,14,16,17,34,35]. Two main effects are used to explain this

improvement: the dynamic Hall-Petch effect and the composite effect, which relates to the co-deformation of the various phases. This second effect seems of particular interest in this case, considering the two levels of heterogeneities discussed before. There is therefore a two-level composite effect observed in this alloy. The first one is an intergranular mechanical contrast between harder grains and softer grains. The second one is the intragranular mechanical contrast, seen between the matrix and the deformation products – harder for twins, softer for martensite. This architectural strain distribution may explain the excellent work-hardening capability and ductility of the alloy.

4 Conclusion

In-situ studies on the heterogeneous nature of deformation in a strain-transformable Ti-V-Cr-Al alloy are reported. The multi-scale analysis of the deformation mechanisms occurring in this alloy allowed to confirm the deformation mechanisms TRIP and TWIP, and the focus is put on the heterogeneity of the different zones of the sample, which depends highly on the grain orientation with respect to the tensile axis. This heterogeneous microstructure results in complementary co-deformation of the material at two different scales (intragranular and intergranular). Finally, with the help of *in-situ* techniques, the behavior of the martensite could be accurately investigated. An important result of this study is that, based on their orientation, grains seem to prefer one or the other deformation mechanism between TRIP and TWIP. Two different behaviors, twinning and martensitic transformation, are thus observed in the primary

stages of the deformation, each of them for a different group of grains. This coincides well with a fast increase of the martensite fraction, found in the form of needles in the grains favorably oriented, that reaches about 30% for ε≈0.12. In the latter stage of the deformation, the overall martensitic content stabilizes, even though it is still formed in small amounts in TWIP-favored grains as secondary mechanism, to accommodate the highly strained areas. These results suggest also that there is, for this alloy, no unique deformation path, but rather two parallel scenarios. It is suggested that the exceptional mechanical properties of this alloy, a yield strength of 420 MPa, a UTS of almost 1200 MPa and a uniform elongation of 35%, can be analyzed as the result of the multi-scale heterogeneities and co-deformation of the various deformation features of this material.

Acknowledgements:

This work was supported by the French Agence Nationale de la Recherche, on the ANR TiTWIP. The authors acknowledge the European Synchrotron Radiation Facility for provision of synchrotron radiation facilities and would like to thank Andy Fitch for assistance in using the beam line ID22.

References

[1] F. Sun, J.Y. Zhang, M. Marteleur, C. Brozek, E.F. Rauch, M. Veron, P. Vermaut, P.J. Jacques, F. Prima, A new titanium alloy with a combination of high strength, high strain hardening and improved ductility, Scr. Mater. 94 (2015) 17–20. doi:http://dx.doi.org/10.1016/j.scriptamat.2014.09.005.

[2] M. Marteleur, F. Sun, T. Gloriant, P. Vermaut, P.J. Jacques, F. Prima, On the design of new β-metastable titanium alloys with improved work hardening rate thanks to

simultaneous TRIP and TWIP effects, Scr. Mater. 66 (2012) 749–752. doi:http://dx.doi.org/10.1016/j.scriptamat.2012.01.049.

[3] C. Brozek, F. Sun, P. Vermaut, Y. Millet, A. Lenain, D. Embury, P.J. Jacques, F. Prima, A β-titanium alloy with extra high strain-hardening rate: Design and mechanical properties, Scr. Mater. 114 (2016) 60–64. doi:http://dx.doi.org/10.1016/j.scriptamat.2015.11.020.

[4] H.Y. Kim, Y. Ikehara, J.I. Kim, H. Hosoda, S. Miyazaki, Martensitic transformation, shape memory effect and superelasticity of Ti–Nb binary alloys, Acta Mater. 54 (2006) 2419–2429. doi:http://dx.doi.org/10.1016/j.actamat.2006.01.019.

[5] T. Grosdidier, M.J. Philippe, Deformation induced martensite and superelasticity in a β-metastable titanium alloy, Mater. Sci. Eng. A. 291 (2000) 218–223. doi:http://dx.doi.org/10.1016/S0921-5093(00)00921-7.

[6] X.H. Min, K. Tsuzaki, S. Emura, K. Tsuchiya, Enhancement of uniform elongation in high strength Ti–Mo based alloys by combination of deformation modes, Mater. Sci. Eng. A. 528 (2011) 4569–4578. doi:https://doi.org/10.1016/j.msea.2011.02.071.

[7] X. Min, X. Chen, S. Emura, K. Tsuchiya, Mechanism of twinning-induced plasticity in β-type Ti–15Mo alloy, Scr. Mater. 69 (2013) 393–396. doi:http://dx.doi.org/10.1016/j.scriptamat.2013.05.027.

[8] R.J. Talling, R.J. Dashwood, M. Jackson, D. Dye, On the mechanism of superelasticity in Gum metal, Acta Mater. 57 (2009) 1188–1198. doi:https://doi.org/10.1016/j.actamat.2008.11.013.

[9] M. Ahmed, D. Wexler, G. Casillas, O.M. Ivasishin, E.V. Pereloma, The influence of β phase stability on deformation mode and compressive mechanical properties of Ti–10V–3Fe–3Al alloy, Acta Mater. 84 (2015) 124–135. doi:https://doi.org/10.1016/j.actamat.2014.10.043.

[10] R.P. Kolli, W.J. Joost, S. Ankem, Phase Stability and Stress-Induced Transformations in Beta Titanium Alloys, JOM. 67 (2015) 1273–1280. doi:10.1007/s11837-015-1411-y.

[11] M. Abdel-Hady, K. Hinoshita, M. Morinaga, General approach to phase stability

and elastic properties of β-type Ti-alloys using electronic parameters, Scr. Mater. 55 (2006) 477–480. doi:http://dx.doi.org/10.1016/j.scriptamat.2006.04.022.

[12] D. Raabe, B. Sander, M. Friák, D. Ma, J. Neugebauer, Theory-guided bottom-up design of β-titanium alloys as biomaterials based on first principles calculations: Theory and experiments, Acta Mater. 55 (2007) 4475–4487. doi:https://doi.org/10.1016/j.actamat.2007.04.024.

[13] M. Besse, P. Castany, T. Gloriant, Mechanisms of deformation in gum metal TNTZ-O and TNTZ titanium alloys: A comparative study on the oxygen influence, Acta Mater. 59 (2011) 5982–5988. doi:http://dx.doi.org/10.1016/j.actamat.2011.06.006.

[14] P. Castany, A. Ramarolahy, F. Prima, P. Laheurte, C. Curfs, T. Gloriant, In situ synchrotron X-ray diffraction study of the martensitic transformation in superelastic Ti-24Nb-0.5N and Ti-24Nb-0.5O alloys, Acta Mater. 88 (2015) 102–111. doi:http://dx.doi.org/10.1016/j.actamat.2015.01.014.

[15] E. Bertrand, P. Castany, I. Péron, T. Gloriant, Twinning system selection in a metastable β-titanium alloy by Schmid factor analysis, Scr. Mater. 64 (2011) 1110–1113. doi:10.1016/j.scriptamat.2011.02.033.

[16] X. Min, S. Emura, X. Chen, X. Zhou, K. Tsuzaki, K. Tsuchiya, Deformation microstructural evolution and strain hardening of differently oriented grains in twinning-induced plasticity β titanium alloy, Mater. Sci. Eng. A. 659 (2016) 1–11. doi:https://doi.org/10.1016/j.msea.2016.01.105.

[17] X. Zhou, X. a Min, S. Emura, K. Tsuchiya, Accommodative 332〈113〉 primary and secondary twinning in a slightly deformed β-type Ti-Mo titanium alloy, Mater. Sci. Eng. A. 684 (2017) 456–465. doi:https://doi.org/10.1016/j.msea.2016.12.025.

[18] X. Ji, S. Emura, X. Min, K. Tsuchiya, Strain-rate effect on work-hardening behavior in β-type Ti-10Mo-1Fe alloy with TWIP effect, Mater. Sci. Eng. A. 707 (2017) 701–707. doi:https://doi.org/10.1016/j.msea.2017.09.055.

[19] X.H. Min, K. Tsuzaki, S. Emura, K. Tsuchiya, Heterogeneous twin formation and its effect on tensile properties in Ti–Mo based β titanium alloys, Mater. Sci. Eng. A. 554 (2012) 53–60. doi:https://doi.org/10.1016/j.msea.2012.06.009.

[20] A.G. Crocker, Twinned martensite, Acta Metall. 10 (1962) 113–122.

doi:10.1016/0001-6160(62)90056-1.

[21] H. Tobe, H.Y. Kim, T. Inamura, H. Hosoda, S. Miyazaki, Origin of 332 twinning in metastable β-Ti alloys, Acta Mater. 64 (2014) 345–355. doi:https://doi.org/10.1016/j.actamat.2013.10.048.

[22] T. Kawabata, S. Kawasaki, O. Izumi, Mechanical properties of TiNbTa single crystals at cryogenic temperatures, Acta Mater. 46 (1998) 2705–2715. doi:https://doi.org/10.1016/S1359-6454(97)00475-8.

[23] M.J. Lai, C.C. Tasan, D. Raabe, On the mechanism of 332 twinning in metastable β titanium alloys, Acta Mater. 111 (2016) 173–186. doi:https://doi.org/10.1016/j.actamat.2016.03.040.

[24] B. Chen, W. Sun, Transitional structure of 332〈113〉β twin boundary in a deformed metastable β-type Ti-Nb-based alloy, revealed by atomic resolution electron microscopy, Scr. Mater. 150 (2018) 115–119. doi:https://doi.org/10.1016/j.scriptamat.2018.03.009.

[25] P. Castany, Y. Yang, E. Bertrand, T. Gloriant, Reversion of a Parent {130}⟨310⟩α" Martensitic Twinning System at the Origin of {332}<113>β Twins Observed in Metastable β Titanium Alloys, Phys Rev Lett. 117 (2016) 245501. doi:10.1103/PhysRevLett.117.245501.

[26] F. Sun, J.Y. Zhang, M. Marteleur, T. Gloriant, P. Vermaut, D. Laillé, P. Castany, C. Curfs, P.J. Jacques, F. Prima, Investigation of early stage deformation mechanisms in a metastable β titanium alloy showing combined twinning-induced plasticity and transformation-induced plasticity effects, Acta Mater. 61 (2013) 6406–6417. doi:http://dx.doi.org/10.1016/j.actamat.2013.07.019.

[27] J. Zhang, C.C. Tasan, M.J. Lai, A.-C. Dippel, D. Raabe, Complexion-mediated martensitic phase transformation in Titanium, Nat. Commun. 8 (2017) 14210.

[28] M.J. Lai, C.C. Tasan, J. Zhang, B. Grabowski, L.F. Huang, D. Raabe, Origin of shear induced β to ω transition in Ti–Nb-based alloys, Acta Mater. 92 (2015) 55–63. doi:https://doi.org/10.1016/j.actamat.2015.03.040.

[29] J.Y. Zhang, J.S. Li, Z. Chen, Q.K. Meng, F. Sun, B.L. Shen, Microstructural evolution of a ductile metastable β titanium alloy with combined TRIP/TWIP effects, J. Alloys Compd. 699 (2017) 775–782.

doi:https://doi.org/10.1016/j.jallcom.2016.12.394.

[30] J. Gao, Y. Huang, D. Guan, A.J. Knowles, L. Ma, D. Dye, W.M. Rainforth, Deformation mechanisms in a metastable beta titanium twinning induced plasticity alloy with high yield strength and high strain hardening rate, Acta Mater. 152 (2018) 301–314. doi:https://doi.org/10.1016/j.actamat.2018.04.035.

[31] C. Brozek, F. Prima, Y. Millet, B. Peltier, Turbomachine part comprising an alloy based on titanium, WO2016066955, n.d.

[32] L. Remy, Kinetics of f.c.c. deformation twinning and its relationship to stress-strain behaviour, Acta Metall. 26 (1978) 443–451. doi:https://doi.org/10.1016/0001-6160(78)90170-0.

[33] M.J. Lai, T. Li, D. Raabe, ω phase acts as a switch between dislocation channeling and joint twinning- and transformation-induced plasticity in a metastable β titanium alloy, Acta Mater. 151 (2018) 67–77. doi:https://doi.org/10.1016/j.actamat.2018.03.053.

[34] S. Hanada, T. Yoshio, O. Izumi, Effect of Plastic Deformation Modes on Tensile Properties of Beta Titanium Alloys, Trans. Jpn. Inst. Met. 27 (1986) 496–503. doi:10.2320/matertrans1960.27.496.

[35] Y. Yang, P. Castany, M. Cornen, F. Prima, S.J. Li, Y.L. Hao, T. Gloriant, Characterization of the martensitic transformation in the superelastic Ti–24Nb–4Zr–8Sn alloy by in situ synchrotron X-ray diffraction and dynamic mechanical analysis, Acta Mater. 88 (2015) 25–33. doi:https://doi.org/10.1016/j.actamat.2015.01.039.

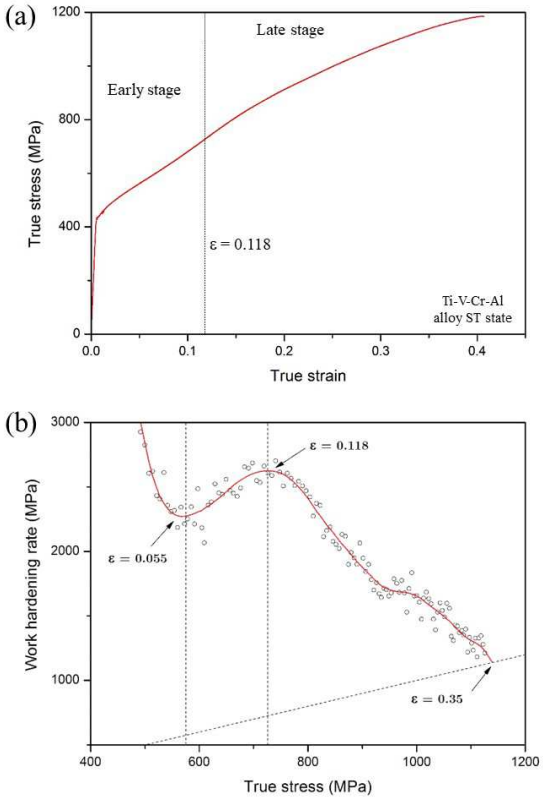

Figure 1: Uniaxial mechanical properties of Ti-V-Cr-Al alloy in the ST state. (a) true stress-true strain curve. (b) Work hardening rate as a function of the true stress.

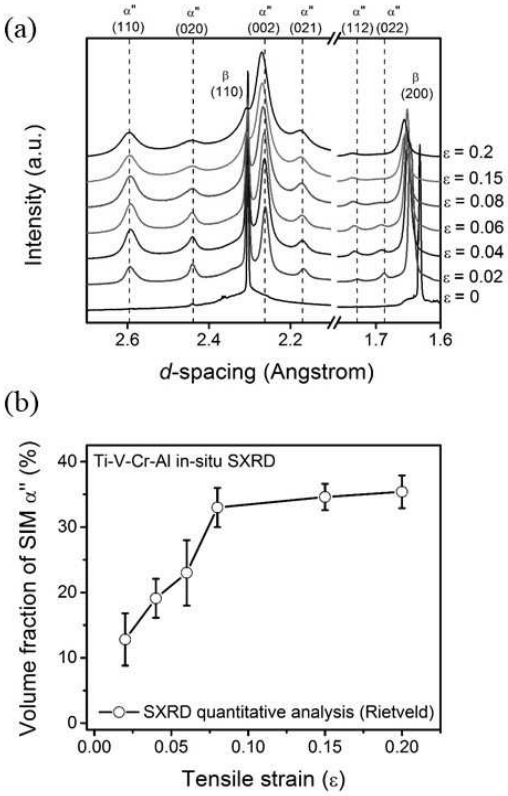

Figure 2: In-situ synchrotron X-ray diffraction (SXRD) upon uniaxial tension. (a) Diffraction patters for strains between 0 and 0.2. (b) Volume fraction of the α" phase (quantified by Rietveld refinement) as a function of the tensile strain.

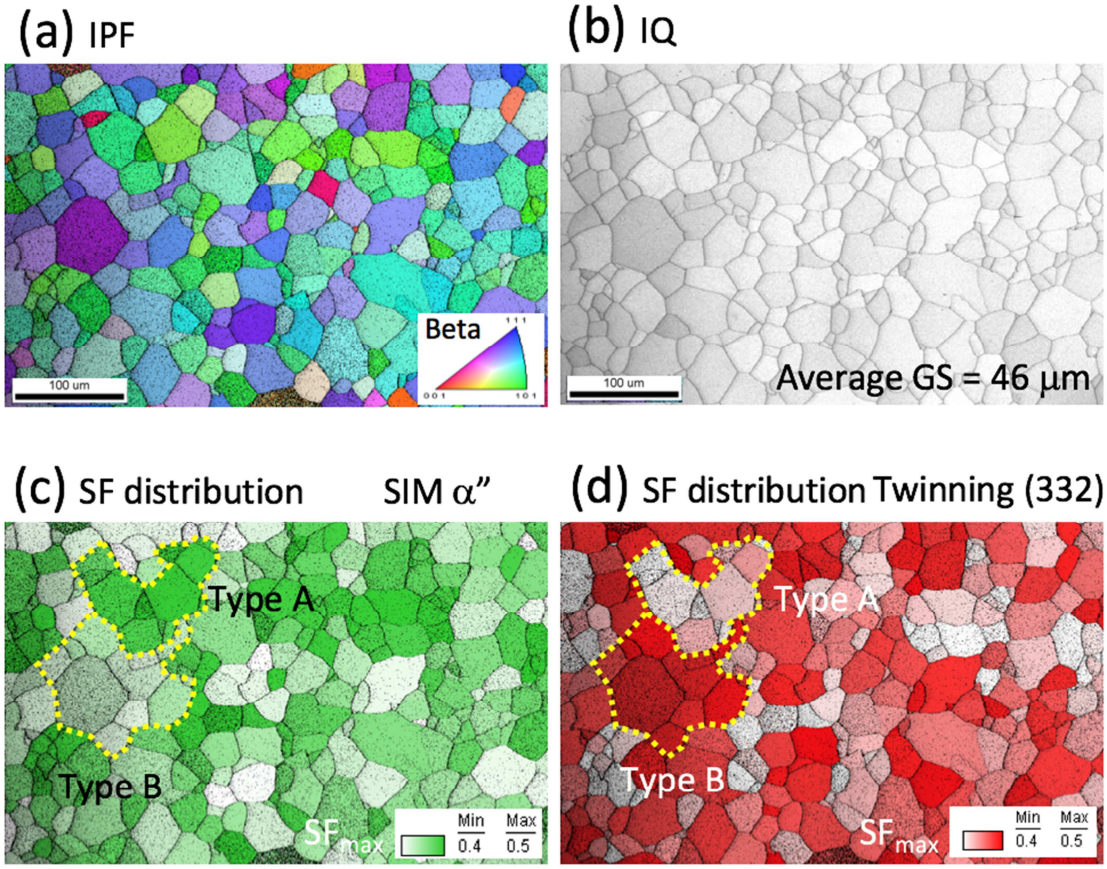

Figure 3: EBSD mapping of the in-situ traction specimen before deformation. (a) Inversed pole figure, IPF. (b) Image quality, IQ. (c) Schmid factor ($0.4<SF_{max}<0.5$) distribution of SIM a" along tensile direction. (d) Schmid factor ($0.4<SF_{max}<0.5$) distribution of {332}<113> twinning system along tensile direction. Examples of groups of Type A grains and Type B are marked by yellow dash lines in (c) and (d).

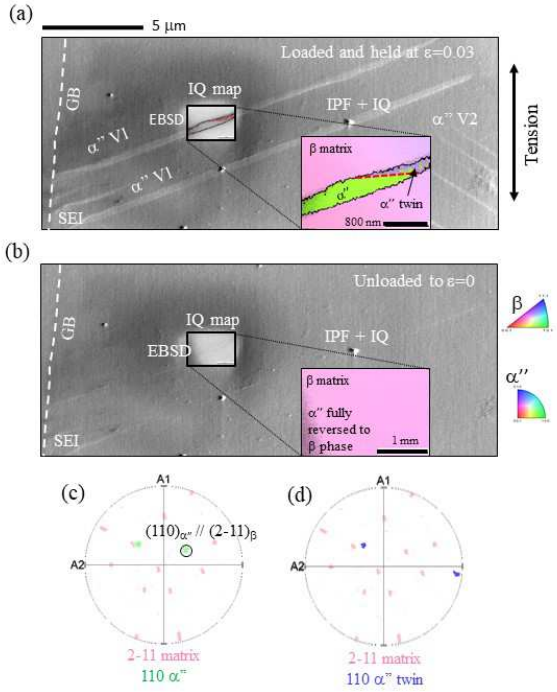

Figure 4: Early stage in-situ investigation grain A. (a) SE imaging and IPF + image quality of the EBSD mapping at ε=0.003 (EBSD recorded in charge). (b) Sample unloaded to ε=0, SE image and EBSD mapping of the same zone. (c) Burgers classical relationship found between the matrix (pink) and the green α" (marked by a black circle). (d) orientations of the α" twin and the matrix, showing no Burgers relationship.

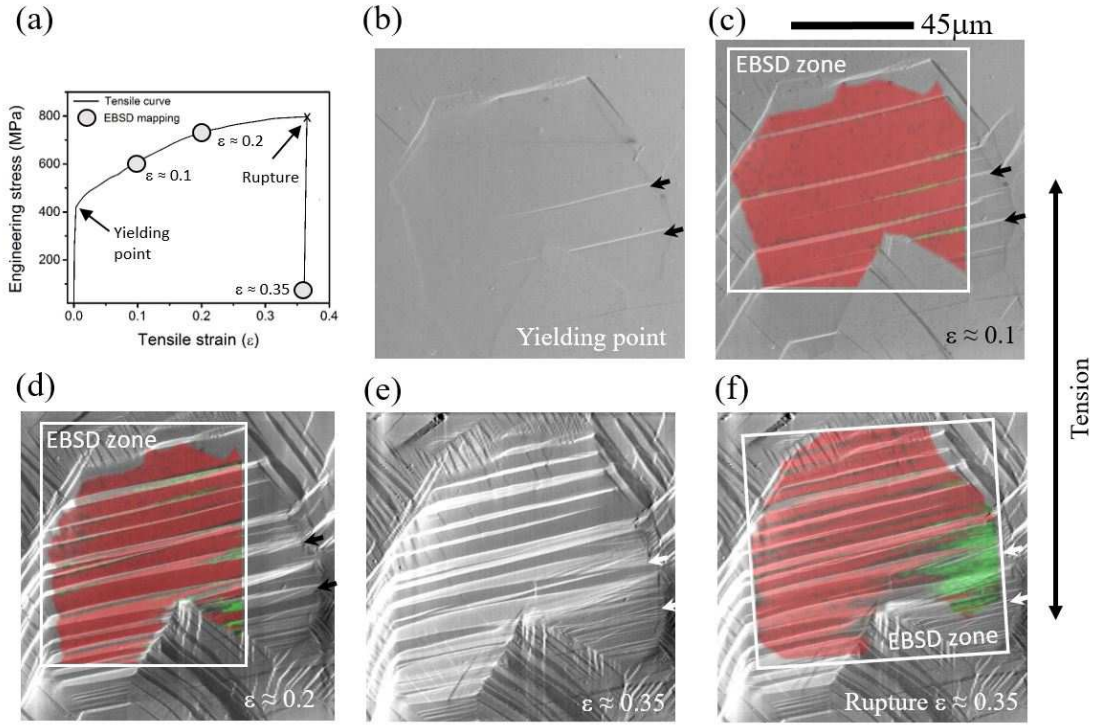

Figure 5: In-situ investigation of the deformation in grain B. (a) corresponding in-situ stress/strain curve. (b-f) SE images at yielding, ε≈0.1, ε≈0.2, ε≈0.35 and after rupture respectively (sample always under charge). The EBSD phase maps are superimposed to the SE images for (c), (d) and (f), with β in red and α" in green.

(a)

β twins 28.2%				β matrix	α'' SIM 10.3%		
System	Area%	Variant	Name		Name	Variant	Area%
{332}<113>	26.1	(3-23)[131]	T1		a1	(5-75)[7 10 7]	2.3
	0.9	(-233)[311]	T2		a2	(575)[7 -10 7]	1.3
	0.2	(323)[1-31]	T3		a3	Detected after rupture	6.6
{112}<111>	0.7	(121)[1-11]	T4				

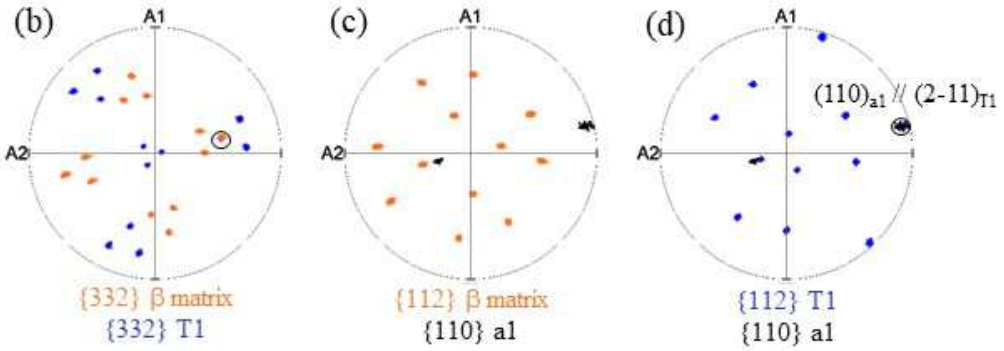

Figure 6: Analysis of the twinning and martensite variants after rupture in grain B. (a) identification, distributions and area fractions of all the variants. (b) {332} planes of the β matrix and T1 showing the twinning plan (black circle). (c) {211} planes of the β matrix and {011} planes of a1 showing no Burgers relationship. (d) {211} planes T1 and {011} planes of a1 displaying the Burgers relationship.

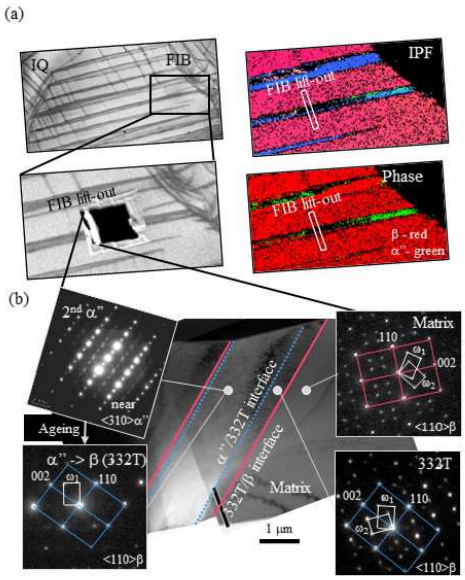

Figure 7: TEM analysis of the profile of a deformation band in grain B. (a) EBSD IQ, IPF and phase map of the band before the liftout. (b) TEM bright field of the band, and diffraction patterns corresponding to the different zones of the band. Twinning interfaces are marked by a red line and interface between α" and the β twin are marked by a blue line.

Products			Schmid factors					
			Grain A		Grain B		T1	
	System	Variant	(hkl)[uvw]	SF	(hkl)[uvw]	SF	(hkl)[uvw]	SF
Twinning	332	1	(3 -2 3)[1 3 1]	0,429	(3 -2 3)[1 3 1]	0,457	(3 -2 3)[1 3 1]	0,453
		2	(3 2 3)[1 -3 1]	0,319	(-2 3 3)[3 1 1]	0,295	(-2 3 3)[3 1 1]	0,372
		3	(-2 3 3)[3 1 1]	0,243	(3 2 3)[1 -3 1]	0,271	(3 2 3)[1 -3 1]	0,177
	112	1	(1 2 1)[1 -1 1]	0,486	(1 2 1)[1 -1 1]	0,484	(1 2 1)[1 -1 1]	0,457
		2	(1 -2 1)[1 1 1]	0,428	(1 -2 1)[1 1 1]	0,392	(1 -2 1)[1 1 1]	0,312
		3	(1 -1 2)[1 -1 -1]	0,13	(2 -1 1)[-1 1 1]	0,191	(2 -1 1)[-1 1 1]	0,295
Martensite		1	(5 -7 5)[7 10 7]	0,486	(5 -7 5)[7 10 7]	0,452	(5 -7 5)[7 10 7]	0,41
		2	(5 7 5)[7 -10 7]	0,484	(5 7 5)[7 -10 7]	0,452	(5 7 5)[7 -10 7]	0,406
		3	(-5 5 7)[7 -7 10]	0,238	(-5 5 7)[7 -7 10]	0,283	(-5 5 7)[7 -7 10]	0,349

Figure 8: Schmid factors and variants of the deformation products of grain A and grain B. The colors correspond to the color-coded orientation of the features on the EBSD IPF images. The (3-23)[131] twin (grey) is detected but not treated in a larger extent as its area fraction is very low.

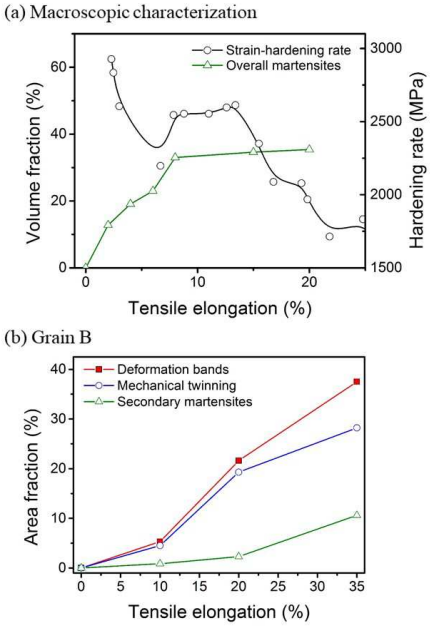

Figure 9: (a) Evolution of the overall martensite volume fraction (SXRD) and the work hardening rate as a function of strain. (b) Evolution of the various deformation features in grain B as a function of strain.